

A Knowledge-Based System for Generation and Control of Finite-Element Meshes in Forging Simulation

P.D. Dabke, I. Haque, M. Srikrishna, and J.E. Jackson

This article presents a two-dimensional mesh generation system designed to generate all quadrilateral meshes for forging applications. The system splits the meshing geometry into a set of "primitives" using a knowledge-based system. It further splits these primitives into quadrilaterals using standard primitive splitting algorithms and meshes each quadrilateral using parametric mapping. Reasons for choosing this approach are explained, followed by a brief description of the implementation procedures. Three mapping techniques—namely, two-dimensional Lagrange interpolation, two-dimensional Hermite interpolation, and numerical solution of Poisson's equation—were tested for their applicability to forging problems. This article provides a comparison of the three mapping techniques in terms of mesh quality and computational time. Finally, it presents results of three forging simulations that demonstrate the effects of element distortion on finite-element solutions of large plastic deformation problems and points out the correlation between distortion parameters such as skew and taper and the solution accuracy.

1. Introduction

SINCEits introduction in metal-forming analysis, the finite-element method has proved to be an effective tool for forging process design. The finite-element analysis provides a detailed picture of the forging process and eliminates the need of adopting an expensive and time-consuming trial and error approach toward forging design. It is commonly recognized that the success of a finite-element simulation of such large plastic strain problems depends on the following factors:

- Choice of the material constitutive relations in the finite-element formulation
- Representation of friction and thermal boundary conditions at the die/workpiece interface
- Numerical factors such as integration schemes, mesh quality in terms of mesh density distribution and element distortion, and remeshing

In the recent past, significant attention has been paid to the first two issues, namely, the representation of the material constitutive relations and simulation of frictional boundary conditions.[1,2] Researchers have also studied the influence of numerical integration schemes on the accuracy of finite-element solutions.[2,3] Little, however, has been done on quantifying the influence of mesh generation schemes, mesh quality, and remeshing on the accuracy of large deformation solutions. Forging simulations are time intensive and costly, typically requiring a few hours of analysis time, even for relatively simple problems. A proper discretization of the workpiece into finite elements is therefore critical to obtaining cost-effective and accurate finite-element solutions and assumes a great importance in forging applications. Normally, mesh generation for these problems is done either manually, which works fairly well for simple shapes, or through the use of built-in capabilities of commercially available packages like PATRAN.* Commercial mesh generators such as PATRAN normally use parametric mapping for mesh generation. Although this option offers a limited improvement over manual mesh generation, the user is still required to define the meshing geometry in terms of mappable patches. Hence, this approach is not fully automated. Mesh generation using this approach is still a tedious task and does not provide a desirable level of flexibility. It is found to be even more tedious when used for remeshing. Our experience also indicates that the analyst needs to have a thorough understanding of the simulation process to produce a good quality mesh giving reliable finite-element results. In short, there is a genuine need for automating mesh generation, because this would result in significant saving in analysis time and would make finite-element analysis accessible to a forging designer relatively inexperienced in finite elements.

This article addresses the development of a knowledge-based system for automating mesh generation and remeshing in large deformation problems. The method presented here was implemented into CFORM,[4] a finite-element package developed for research purposes, to simulate plane-strain and axisymmetric material flow in hot forming operations for conventional and powdered metals. CFORM is based on a rigid thermoviscoplastic formulation, as are other well-known computer codes such as ALPIDT.[5] It is currently being extended to the forming of whisker-reinforced metal matrix composites.[6] This article first discusses the structure of the knowledge-based system with a brief description of the mesh generation algorithm and the implementation details. The system produces two-dimensional all-quadrilateral meshes, because they are generally found to be computationally more reliable,[7] and provides a framework for controlling the mesh parameters. The system is based on the mapped mesh generation approach and tests three parametric mapping methods, namely two-dimensional Lagrange interpolation, two-dimensional Hermite interpolation, and numerical solution of Poisson's equation, for their applicability to forging analysis. This article provides a comparison between the three mapping techniques in terms of element distortion and computational time. Finally, the effect

P.D. Dabke, I. Haque, and **M. Srikrishna**, Department of Mechanical Engineering, Clemson University, Clemson, South Carolina; and **J.E. Jackson**, Department of Aerospace Engineering, University of Alabama, Tuscaloosa, Alabama.

*PATRAN is a registered trademark of PDA Engineering.

of element distortion on finite-element solutions in large plastic strain problems is discussed by presenting results of three forging simulations.

2. Mesh Generation Approach

A number of methods are available in the literature for generation of finite-element meshes. Mesh generation methods, commonly used today for two-dimensional problems, can be classified into four approaches:[8,9]

- Node placement followed by element generation
- Element generation by nodal subdivision
- Mesh generation by spatial subdivision (quadtree methods)
- Mesh generation by parametric space mapping

The first approach[10,11] is able to generate either an all triangular mesh, or a mixture of triangles and quadrilaterals,[8] but does not guarantee an all quadrilateral mesh. Amongst the other three, the mapped mesh approach was selected for implementation, for the following reasons. Mapped mesh generation produces better shaped quadrilateral elements at the boundary with a regular pattern of connectivity, compared to other mesh generation techniques. These techniques [12-15] sometimes result in distorted and very small boundary elements. The distortion in the boundary elements is an important concern in forging analysis. High stress/strain gradients are often expected near the workpiece boundary. The element stresses near the boundary are directly related to the die stresses and forging loads. Thus, distortion in the boundary elements would have an adverse effect on the accuracy of prediction of forging parameters such as peak stresses and loads. Mapped mesh generation methods have a lower computational cost than the other two approaches.

The mesh generation system developed here utilizes parametric mapping in conjunction with a knowledge-based approach, suggested by T.D. Blacker *et al.*[16,17] It first splits the two-dimensional geometry to be meshed into meshable patches. These patches, also called primitives, are decomposed further into quadrilaterals, using standard primitive decomposition algorithms. Finally, each of these quadrilaterals is meshed using a parametric mapping technique. The reasons for adopting this approach are as follows. The knowledge-based system automates the task of splitting the meshing geometry into mappable patches. This minimizes the user interaction and allows complete automation of the mesh generation process. A knowledge-based approach focuses on a narrow domain of meshing problems (*i.e.*, geometries encountered in forging analysis). Although this limits the use of the mesh generation system to a specific class of problems, it is much cheaper and more efficient than other approaches that try to mesh arbitrarily complex geometries. The knowledge-based system can be extended to automate other knowledge intensive tasks such as material selection, determination of time step size, remeshing, etc.

The mesh generation approach used here is adequately described in Ref 16 and will not be described in detail. The knowledge representation and dissection strategies are unique to this work and are described in detail in the next section. The algorithmic procedure for implementing these strategies is as follows:

1. Read the input geometry and compute interior angles at the region vertices.
2. Group the vertices into five classes according to their interior angles. Three of the classes include vertices that are classified exclusively as corners, side, or dissection vertices. The other two classes include (1) vertices that can be treated as corners or as side vertices and (2) vertices that can be treated as side or dissection vertices.
3. Test the region to see if it is simple, or needs to be dissected. A region is considered simple if (1) the number of corner vertices is between 2 and 5, (2) there is no dissection vertex, and (3) the region can be interpreted as a primitive providing acceptable mesh quality.
4. If the region is not simple, dissect it into two subregions, such that at least one subregion is simple. If the other subregion is also simple, proceed to Step 5; otherwise dissect the other subregion recursively until all the subregions formed are simple.
5. Split each primitive into quadrilaterals and mesh each quadrilateral using parametric mapping.

3. Mesh Generation System

The meshing system consists of two modules. The first module, written using PROLOG and C, is a knowledge-based system for splitting a given two-dimensional geometry into meshable primitives. This module writes the primitive information in a text file, which serves as an input file for the second module. The second module consists of a set of FORTRAN subroutines for splitting the primitives further into quadrilaterals and meshing them using a parametric mapping method. An outline of the two modules is presented below. More details about the meshing system can be found in Ref 18.

3.1 *PROLOG Module*

A flowchart depicting the primitive generation algorithm is shown in Fig. 1. The knowledge representation strategy adopted in this module is a combination of rule-based and frame-based reasoning.[19,20] The procedural part of the system is programmed as a set of PROLOG rules and makes use of the built-in inference engine provided by PROLOG. Facts, describing the geometry of the region being decomposed, appear as "frames". The system defines the following generic frames for describing the geometry:

- Point
- Segment
- Primitive
- Region

A point is defined by its coordinates. A segment can be either a straight line or a circular arc. All the segments are defined as vectors. A straight segment is defined by its end points. An arc

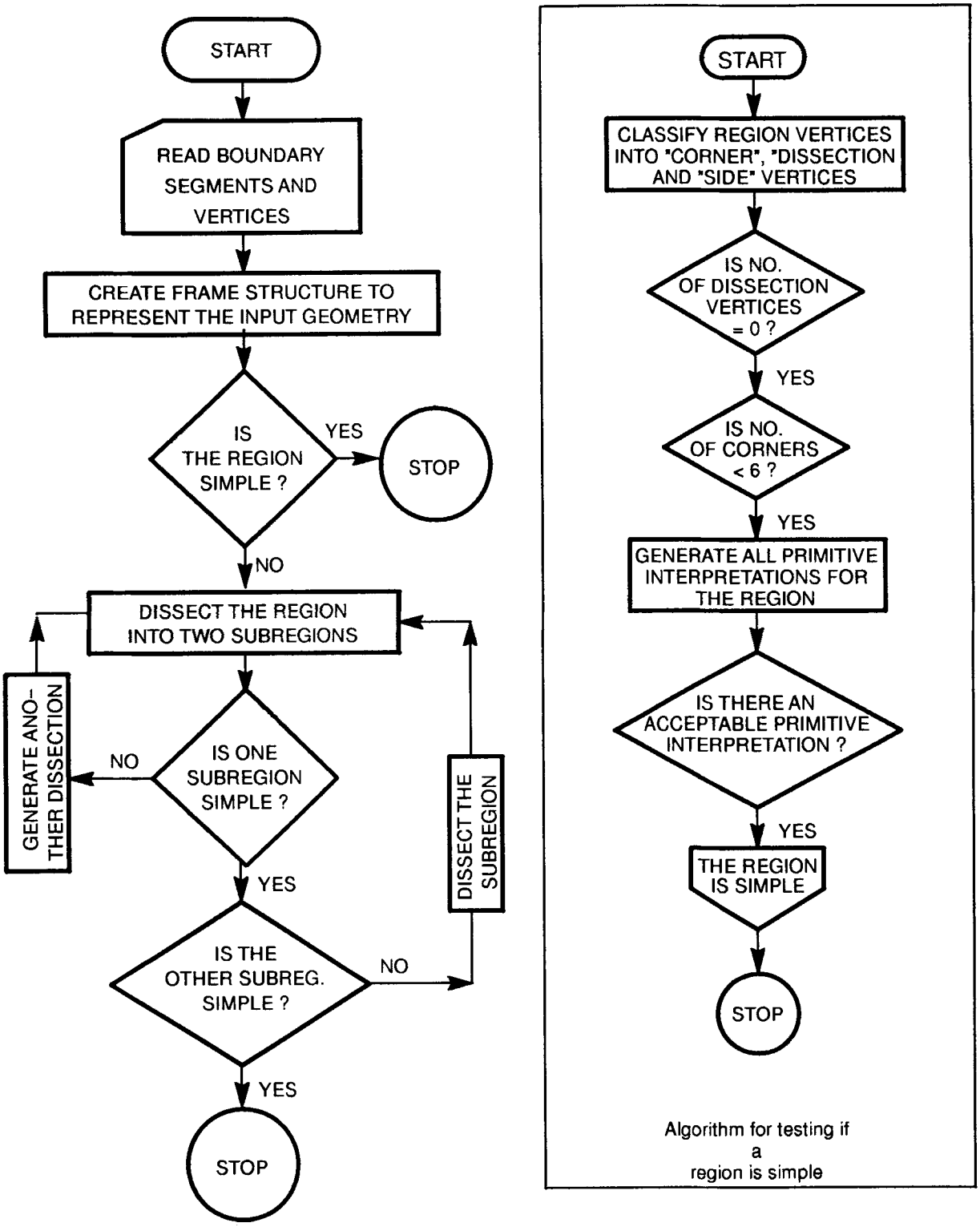

Fig. 1 Primitive generation algorithm.

is defined by its end points, coordinates of the center, and its type (concave/convex). A primitive can be a quadrilateral, a pentagon, a triangle, or a semicircle. A region is defined by its vertices. The geometric entities described above form the basic frame structure of any meshing problem. At the beginning of execution, the inverted tree representing the hierarchical frame structure appears as shown in Fig. 2. After reading the geometric input for the region to be meshed, the program creates instances representing region vertices and boundary segments. As the decomposition proceeds, new instances, representing the dissection segments and points created by the program, are added to the tree. An example of the resulting tree at the end of execution is shown in Fig. 3.

Four dissection strategies have been used to decompose a region into a set of meshable primitives. These strategies are:

- **Vertex angles greater than 300°:** This strategy tries to convert sharp concave vertices into two-sided vertices. In the first step, all boundary segments perpendicular to either of the boundary segments forming the dissection angle within a certain tolerance are found. In the next step, only those segments are considered that intersect with the perpendicular drawn from the dissection vertex. Finally, the shortest perpendicular is chosen as the dissection segment.
- **Angles greater than 210 °:** This strategy consists of drawing a perpendicular from a vertex on a boundary segment parallel (within a certain tolerance) to the segments forming the dissection vertex and having the opposite sense of direction. If the angle is closer to 210°, the dissection will produce two corner vertices. If the angle is closer to 270°, the dissection will produce a corner and a side vertex, and if the angle is more than 300°, the dissection will result in a corner and a dissection vertex.
- **Large convex arcs:** End points of the convex arcs that are close to a semicircle are joined by a dissection segment to produce a semicircle with corners having angles close to 90°.
- **Concave arcs:** This strategy tries to find a straight boundary segment parallel to the tangent at the midpoint of the concave arc. This strategy results in a dissection segment with excellent corners at both ends.

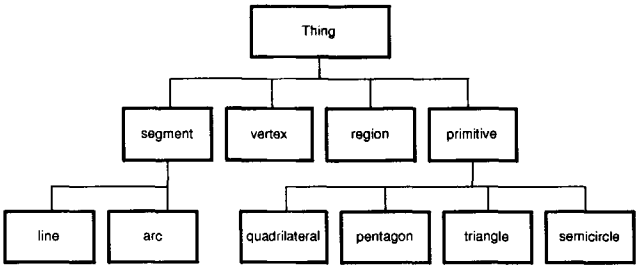

Fig. 2 Initial frame structure.

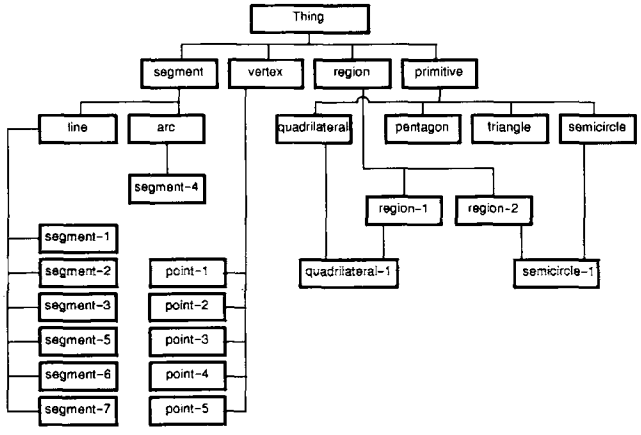

Fig. 3 Frame structure at the end of decomposition.

3.2 *FORTRAN Module*

The FORTRAN module starts its execution after the input geometry has been split into acceptable primitives. It reads the primitive definition and connectivity data, one primitive at a time, identifies the type of primitive, and calls an appropriate subroutine for meshing it. A pentagon and triangles are split into three quadrilaterals. Semicircles are split into two triangles, and each triangle is meshed using the triangle decomposition routine.

The final step in the mesh generation process is meshing individual quadrilaterals, using a parametric mapping technique. The system offers three options for meshing the quadrilaterals:

- Two-dimensional Lagrange interpolation
- Two-dimensional Hermite interpolation
- Numerical solution of Poisson's equation

The first two methods are algebraic interpolation procedures and extend the use of unidirectional Lagrange and Hermite functions to two dimensions. Hermite interpolation allows specification of the first derivative of the function and the two-dimensional interpolation uses this fact to impose orthogonality at the boundary. The third method generates the nodal coordinates by solving Poisson's equation. The form of Poisson's

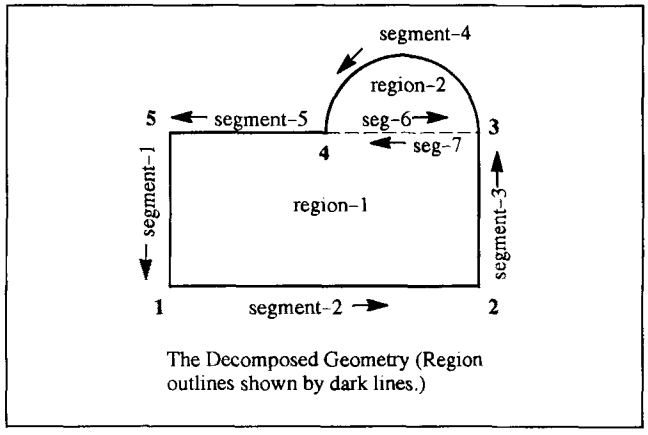

The Decomposed Geometry (Region outlines shown by dark lines.)

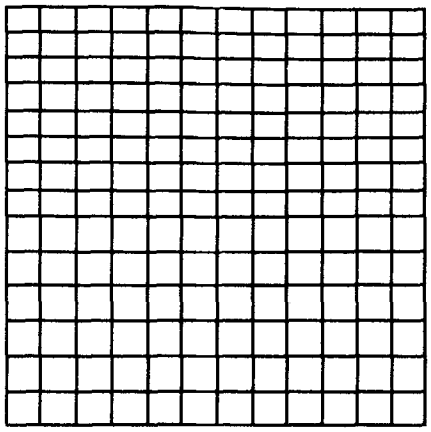

(a)

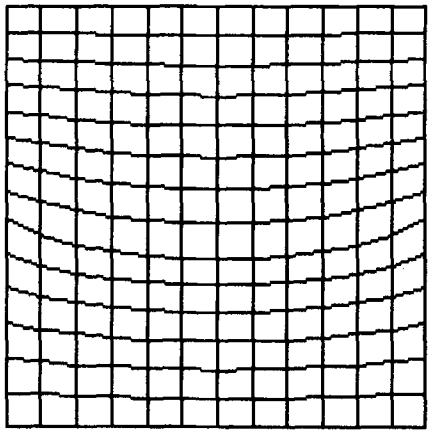

(b)

Fig. 4 Initial mesh for cylinder upsetting. (**a**) Algebraic interpolation. (**b**) Poisson's equation solver.

equation used here is suggested by Thompson *et al.*[21] and is given as follows:

$$\nabla^2\xi = \frac{g_{22}}{g}P \qquad [1]$$

$$\nabla^2\eta = \frac{g_{11}}{g}Q$$

The corresponding equations to be solved to obtain the mesh coordinates are:

$$g_{22}\left(x_{\xi\xi} + Px_{\xi}\right) + g_{11}\left(x_{\eta\eta} + Qx_{\eta}\right) - g_{12}x_{\xi\eta} = 0 \qquad [2]$$

$$g_{22}\left(y_{\xi\xi} + Py_{\xi}\right) + g_{11}\left(y_{\eta\eta} + Qy_{\eta}\right) - g_{12}y_{\xi\eta} = 0$$

where

Table 1 Computational Time (on Sun Workstation) for Meshes Shown in Fig. 9

Mapping method	User time, sec
Lagrange	2.9
Hermite	3.2
Poisson	3.6

$$g_{11} = x_{\xi}^2 + y_{\xi}^2 \qquad g_{22} = x_{\eta}^2 + y_{\eta}^2$$

$$g_{12} = x_{\xi}x_{\eta} + y_{\xi}y_{\eta} \qquad g = \left(x_{\xi}y_{\eta} - x_{\eta}y_{\xi}\right)^2$$

Here, (ξ,η) are the parametric coordinates; (x,y) are the physical coordinates; and the subscripts denote differentiation. P and Q are called control functions because their values can be adjusted to control the grid line spacing and intersection angles in the mesh. In Laplacian smoothening, both P and Q are equal to zero. The numerical equation solver uses two-sided difference approximations for points within the boundary and one-sided difference approximations for the boundary points for calculating partial derivatives. The mesh coordinates are obtained by iteratively solving Eq 2 and adjusting control function values in each iteration so as to obtain orthogonality at the boundary.

Most mapped mesh generators use two-dimensional Lagrange interpolation, also called transfinite interpolation, to generate an initial guess and generate the final mesh using Laplacian smoothening. Hermite interpolation allows the specification of first derivative of the function being interpolated. This is used to impose orthogonality at the mesh boundary, and therefore, this method was expected to offer an improvement over Lagrange interpolation. Laplacian smoothening is equivalent to a numerical solution of Laplace's equation. Poisson's equation reduces to Laplace's equation when both the control functions are zero. It can be mathematically proved[21] that Laplace's equation cannot yield orthogonality at the boundary, if the boundary point distribution is not uniform. As pointed out earlier, the element shape at the boundary is an important issue, and Poisson's equation was expected to provide better meshes in this respect.

4. Comparison of Mapped Mesh Generation Methods

A number of geometries were meshed using the three mapping methods mentioned in the previous section. The mesh topology was preserved in each case so as to make a fair comparison. The three mapping methods were compared on three points—namely, element shapes at the boundary, overall smoothness, and computational time. The remainder of this section is devoted to the discussion of these three points.

The first point for comparison is the shape of the boundary elements. Element shapes produced by Poisson's equation solver are the worst of the three. The other two methods produce much better meshes in this respect. In more complex shapes, Hermite interpolation has been observed to yield better

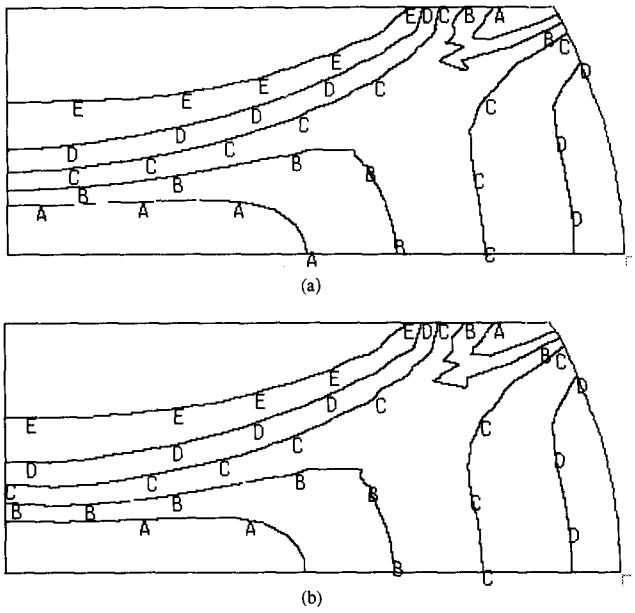

Fig. 5 Effective strain contours at the 44th time step for: cylinder upsetting. **(a)** Algebraic interpolation. **(b)** Poisson's equation solver. (A = 0.9, B = 0.75, C = 0.6, D = 0.45, E = 0.3.)

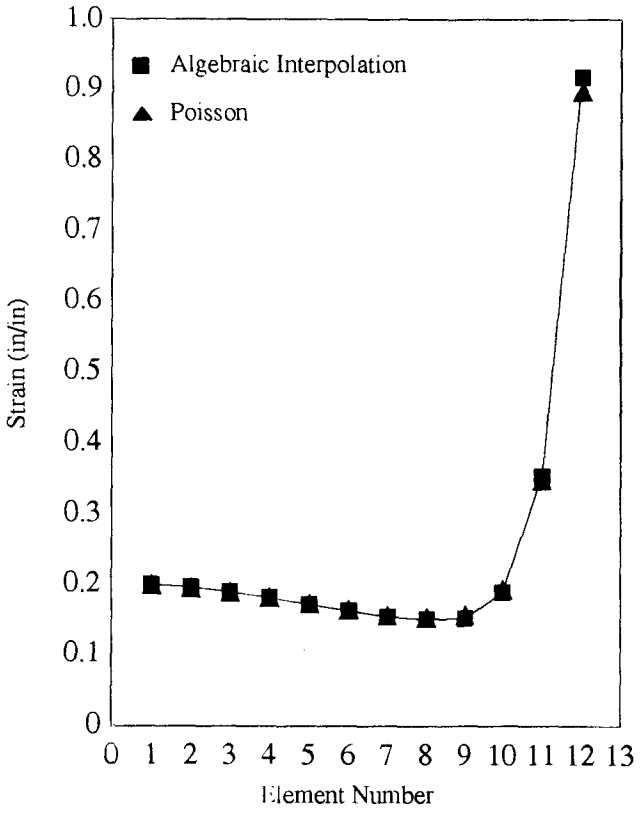

Fig. 6 Effective strain distribution in the elements in contact with the upper die (cylinder upsetting, time step No. 44).

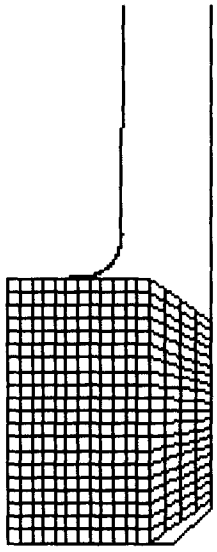

Fig. 7 Initial die and billet configuration for center punch forging.

mesh angles than Lagrange interpolation. The poor quality of Poisson's meshes results from the tendency of elliptical equation solvers to produce uniformly spaced grid lines. This is especially noticeable in Fig. 4(a). Here, the element length changes along the vertical boundaries, but the horizontal grid lines are almost equally spaced in the middle, resulting in a very skewed mesh near the vertical boundaries. Two measures are suggested to alleviate this problem. First, boundary nodes should be placed in a manner that avoids an abrupt change in the element length along the boundary. Second, a better approximation needs to be used in the calculation of the control functions P and Q.

The second point is the overall smoothness of the mesh. The Poisson's equation solver produces the best meshes in terms of overall smoothness, suggesting that use of this technique with a smooth boundary point distribution might prove to be the best strategy for mesh generation. Once again, the other two methods yield comparable results, with Hermite interpolation giving slightly better mesh quality.

The third point for comparison is the computational time needed for mesh generation. The Lagrange interpolation method is the quickest and the Poisson's equation solver the slowest. Computational time required by each method to mesh the geometry shown in Fig. 9 are given in Table 1.

The next two sections present results of three axisymmetric forging simulations performed using the finite-element module of CFORM, which make use of this mesh generation system. These forging cases are (1) cylinder upsetting, (2) center punch forging, and (3) H-section preform. The first section gives the simulation details and the corresponding finite-element results. The next section compares the three mapping methods in terms of distortion parameters such as skew, tapers, aspect ratio, etc., and discusses the effect of mesh distortion on finite-element results.

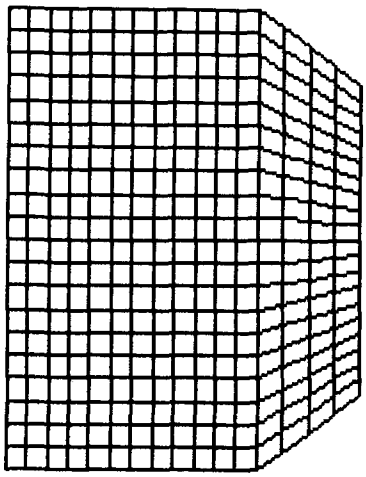

(a)

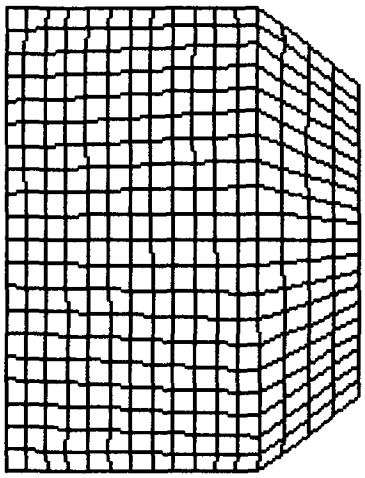

(b)

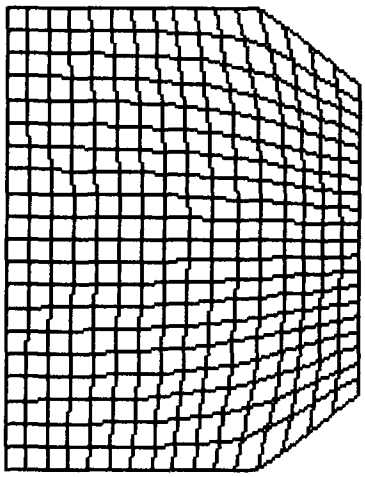

(c)

Fig. 8 Initial mesh for center punch forging. (a) Lagrange. (b) Hermite. (c) Poisson.

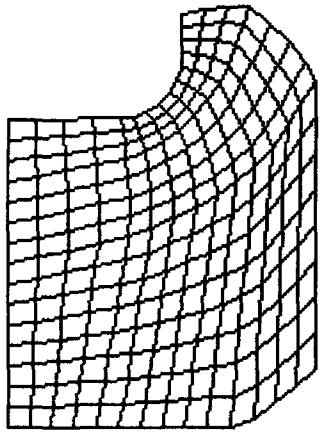

(a)

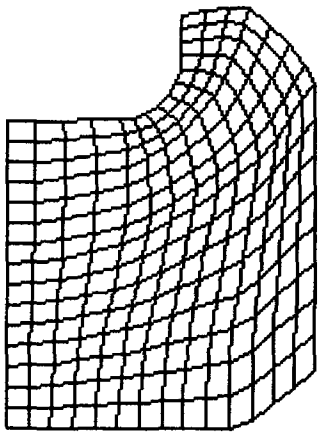

(b)

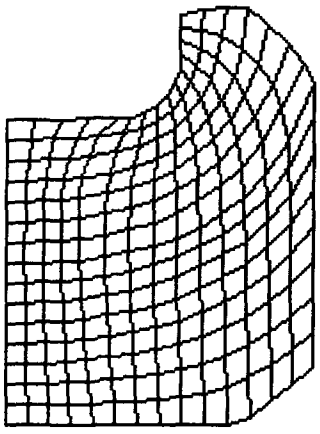

(c)

Fig. 9 New mesh after remeshing at time step No. 40 (center punch forging).

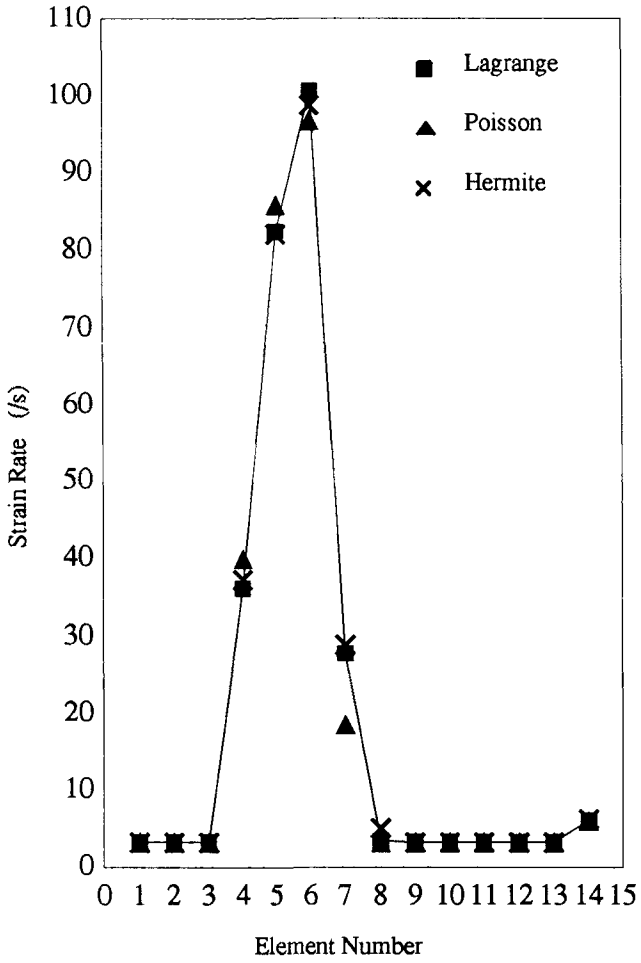

Fig. 10 Effective strain rate distribution in the elements in contact with the moving die (center punch forging, time step No. 40).

5. Details of Forging Simulations

5.1 *Cylinder Upsetting*

The initial height-to-diameter ratio of the cylinder was chosen to be 1.0. The material was assumed to be rigid perfectly plastic, with a yield point of 15,000 psi. Friction between the die and the billet was assumed to be proportional to the normalized radius, with a proportionality constant of 0.3. Only the top right cross section of the cylinder was discretized due to symmetry of the problem. The two algebraic interpolation methods yield identical meshes. The analysis was done using a 7 by 6 element mesh and a 14 by 12 element mesh. The meshes generated in the latter case are shown in Fig. 4. The finite-element results were compared after time step 44, with those obtained by Kobayashi[22] for an identical problem. The effective strain distribution at the 44th time step is shown in Fig. 5. Both mapping methods are observed to yield closely matching results with those in Ref 22 for both mesh configurations. A plot of effective strain in individual elements against element number, for the elements in contact with the upper die, is shown in Fig. 6. Once again, both mapping methods are observed to be in close agreement with each other.

5.2 *Center Punch Forging*

The die geometry and initial and final mesh configurations for this case are shown in Fig. 7, 8, and 9. The material was assumed to be rigid viscoplastic, with an initial yield point of 20,700 psi. A constant shear friction factor of 0.095 was used to incorporate the friction at the die/workpiece interface. The stress-strain rate relationship was assumed to be strain dependent and five stress-strain rate tables, each corresponding to a specific strain value, were used to calculate the appropriate material constants in the analysis. More details about this simulation can be found in Ref 23.

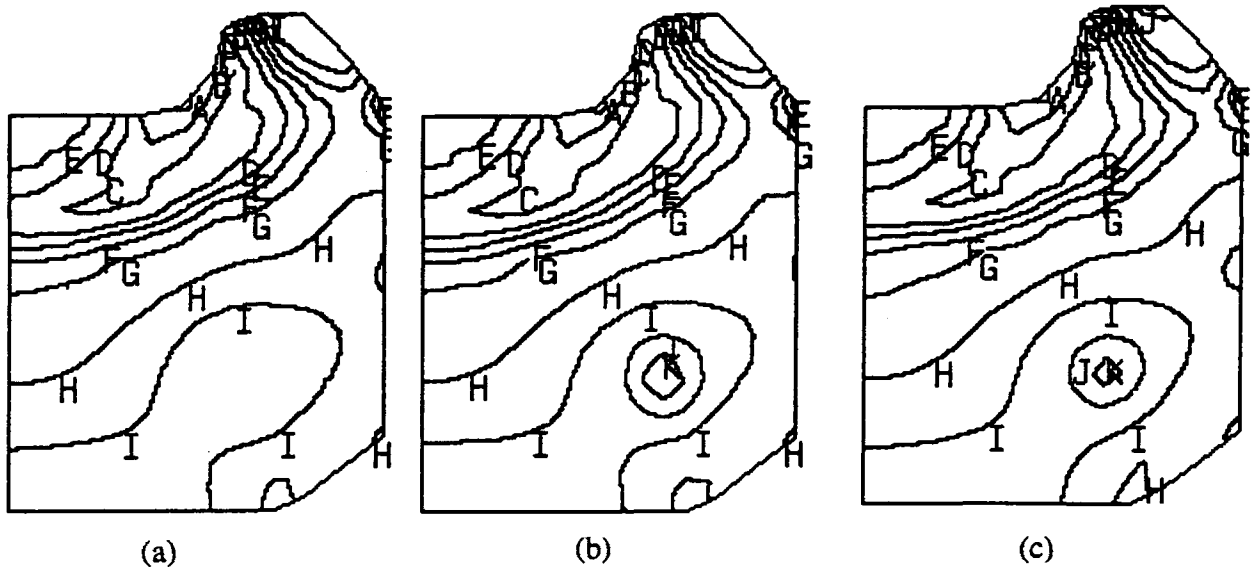

Fig. 11 Effective stress contours at time step No. 30 (center punch forging). (a) Lagrange. (b) Hermite. (c) Poisson; A = 43,500; B = 41,500; C = 39,500; D = 37,500; E = 35,500; F = 33,500; G = 31,500; H = 29,500; I = 27,500; J = 25,500; K = 23,500. All values are in psi.

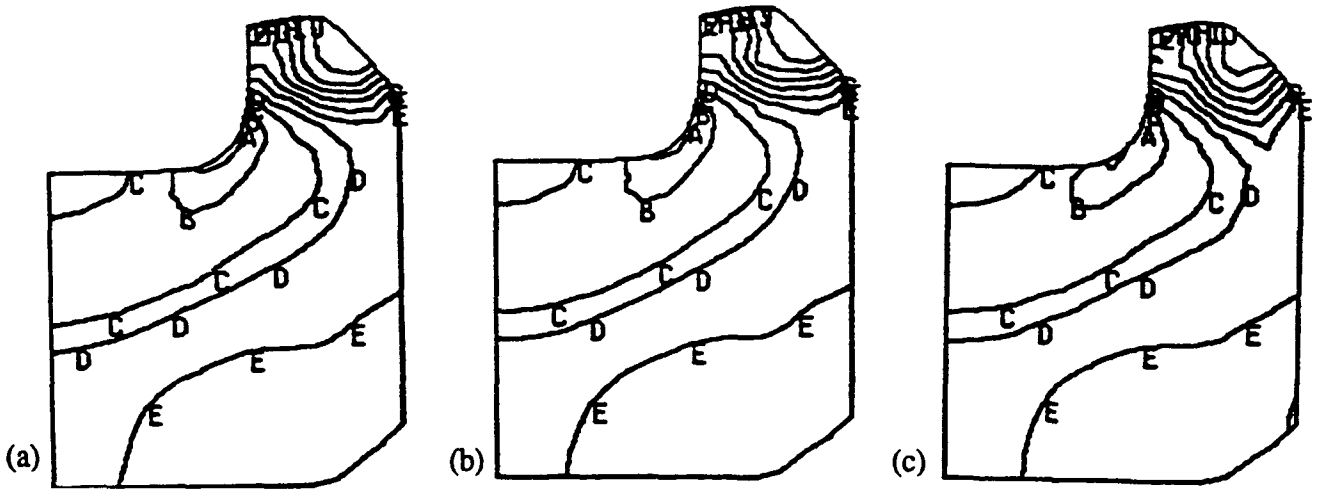

Fig. 12 Effective stress contours at time step No. 50 (center punch forging). **(a)** Lagrange; **(b)** Hermite; **(c)** Poisson; A = 44,500; B = 40,500; C = 36,500; D = 32,500; E = 28,500; F = 24,500; G = 20,500; H = 16,500; I = 12,500; J = 850. All values are in psi.

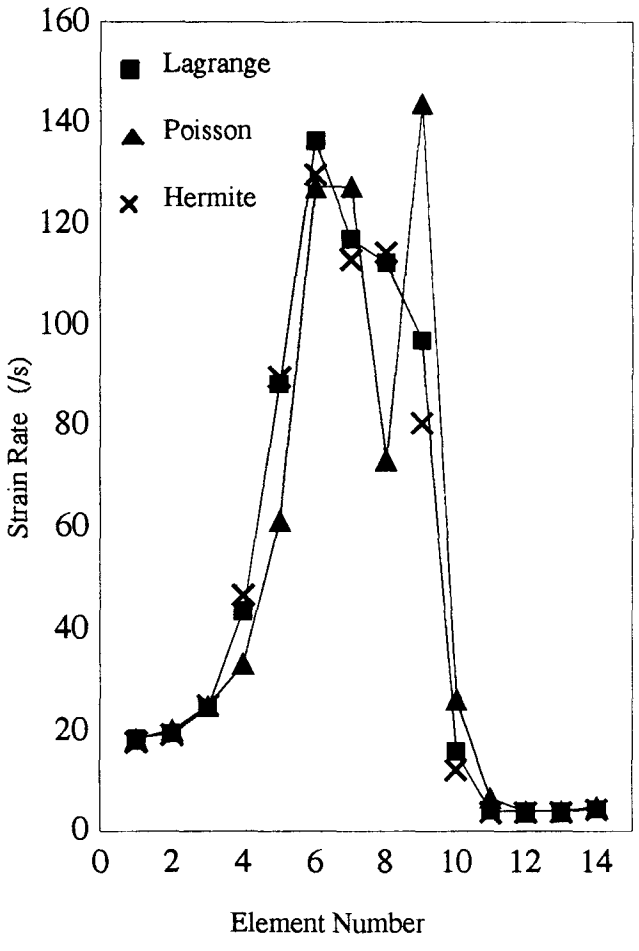

Fig. 13 Effective strain rate distribution in the elements in contact with the moving die (center punch forging, time step No. 50).

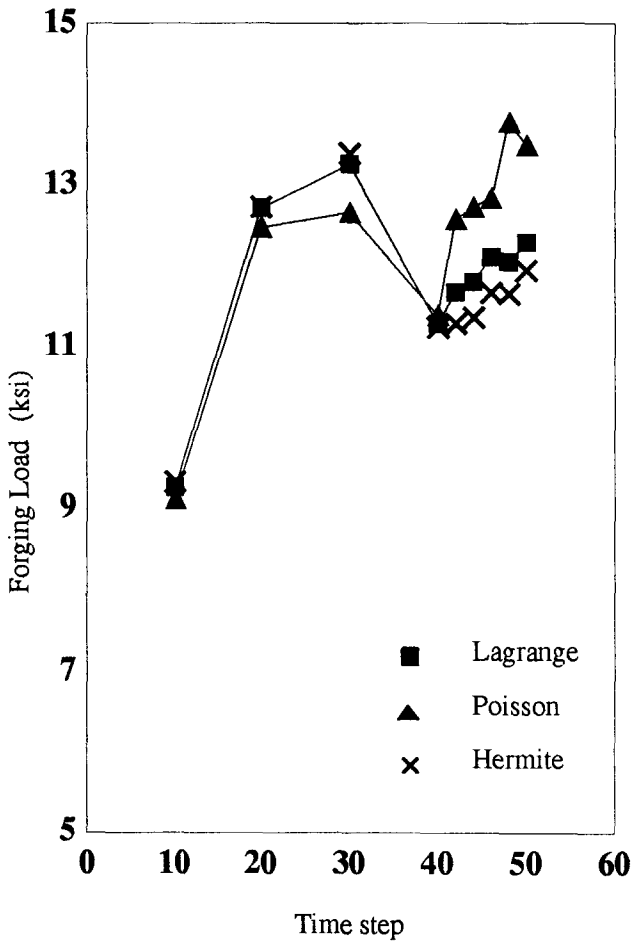

Fig. 14 Forging load versus load step (center punch forging).

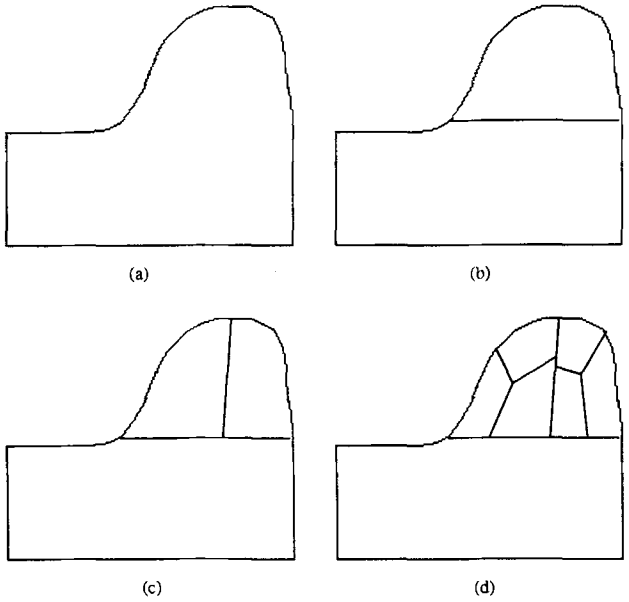

Fig. 15 Decomposition of the meshing geometry into mappable patches. **(a)** Original geometry. **(b)** Decomposition into two primitives. **(c)** Semicircle decomposition. **(d)** Decomposition into seven mappable patches.

The analysis was done for up to 50 time steps, with a uniform time step size of 3×10^{-4} sec. This corresponds to about 50% of the total die stroke. Two mesh configurations, one with 210 elements and 240 nodes and another with 320 elements and 357 nodes, were tried for up to the 40th time step for all three mapping techniques. Neither configuration showed any significant difference in the finite-element results even after the 40th time step. A plot of elemental strain rate variation in the row of elements touching the upper die at time step No. 40 is shown in Fig. 10. In this plot, the element numbering starts from the element in the top left corner. The effective stress contour plots, for the latter case, at time step No. 30 are shown in Fig. 11. Remeshing was done at time step No. 41, and the analysis was continued until the 50th time step, using a new mesh consisting of 210 elements and 240 nodes. The stress contour plots at time step No. 50 are shown in Fig. 12. The elemental strain rate plot at the 50th time step is shown in Fig. 13. A plot of forging load against the time step is shown in Fig. 14.

Until the remeshing step, there is little difference in the results produced by the three mapping methods, and the contour plots as well as the elemental strain plot show close agreement. The contour plots at time step No. 50 also compare very well. The difference becomes noticeable in the elemental strain rate plot shown in Fig. 13. The forging loads also start deviating from time step No. 40. In general, the results obtained using the meshes produced by the algebraic interpolation methods are close, throughout the analysis. The meshes produced using Poisson's equation solver yield results that are markedly different from the other two methods, particularly after the remeshing step.

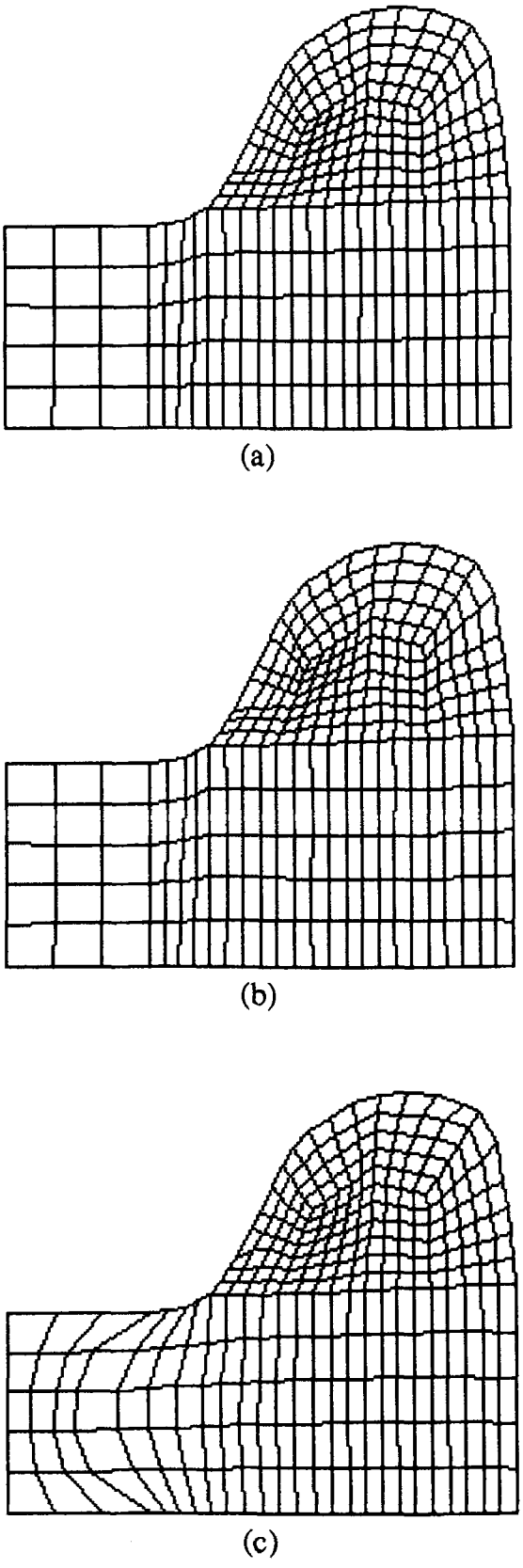

Fig. 16 New mesh after rezoning at time step No. 191 (H-section preform). **(a)** Lagrange. **(b)** Hermite. **(c)** Poisson.

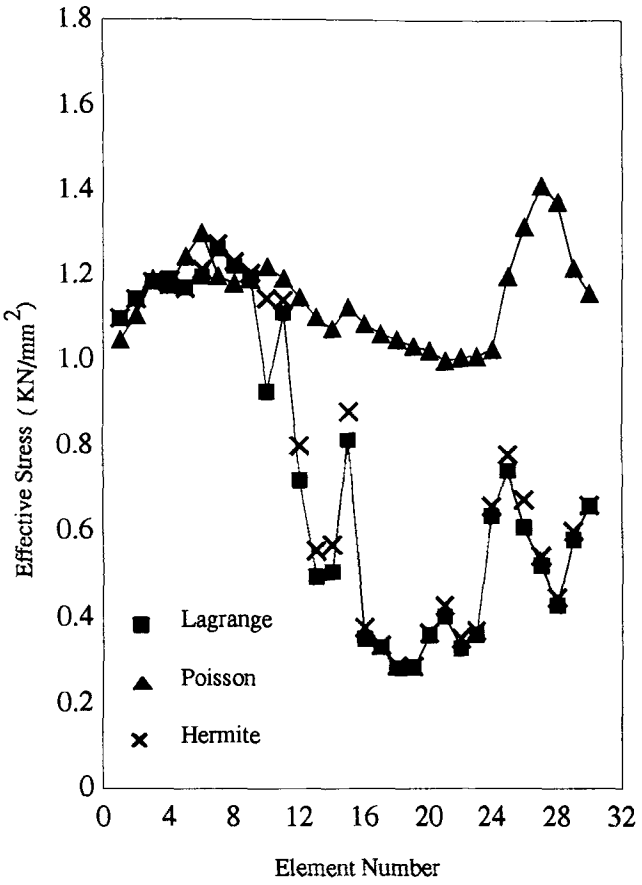

Fig. 17 Effective stress distribution in the elements in contact with the moving die (H-section preform at die closure).

5.3 *H-Section Preform*

The H-section preform analysis began with a cylindrical billet. The material was assumed to be rigid viscoplastic. Stress-strain rate relation was assumed to be independent of strain, and one stress-strain rate table was used to incorporate material properties. A constant shear friction factor of 0.3 was used to model friction. The first remeshing was done at time step No. 91. This corresponds to about 38% of the total die stroke. The initial mesh, as well as the new mesh after remeshing, was generated using Lagrange interpolation. The second remeshing was performed after time step No.191, which corresponds to approximately 70% of the total die stroke. The workpiece geometry was decomposed into two primitives: a semicircle and a quadrilateral, and was meshed using the three mapping methods. The decomposition process is illustrated in Fig. 15. The meshes produced by the three mapping methods after remeshing are shown in Fig. 16. The analysis was continued until die closure. Figure 17 shows an elemental stress plot for the elements in contact with the moving die. The element numbers in this plot start with the element at the top left corner of the billet and proceed along the top row of elements touching the upper die, up to the element at the bottom right corner. The effective stress contours at die closure are shown in Fig. 18.

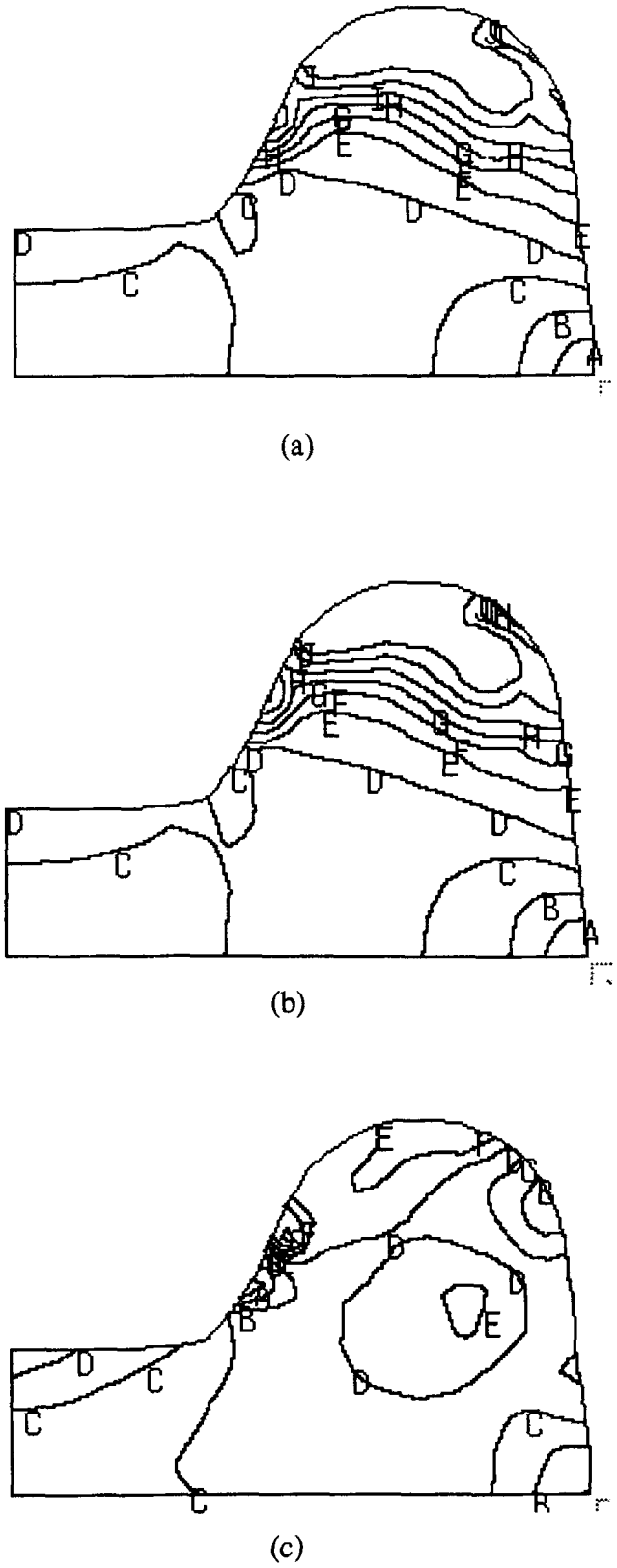

Fig. 18 Effective stress contours at die closure (H-section preform). (a) Lagrange; (b) Hermite; (c) Poisson; A = 1400; B = 1300; C = 1200; D = 1100; E = 1000; F = 900; G = 800; H = 700; I = 600; J = 500. All values are in N/mm^2.

Table 2 Average Distortion Parameters in Cylinder Upsetting

Distortion parameter	Lagrange	Hermite	Poisson
Taper in x direction	7.1429E-09	7.1429E-09	1.5918E-02
	0	0	9.6706-03
Taper in y direction	7.1429E-09	7.1429E-09	1.5919E-02
	0	0	9.6706E-03
Skew	7.1429E-09	7.1429E-09	8.2733E-02
	0	0	7.6910E-03
Aspect ratio	1.1905	1.1905	1.1892
	1.3333	1.3333	1.2386

Note: Two averages are given for each distortion parameter. The first row gives an average for the entire mesh, and the second row gives an average value of the boundary elements in contact with the moving die.

Table 3 Average Distortion Parameters in Center Punch Forging of Initial Mesh

Distortion parameter	Lagrange	Hermite	Poisson
Taper in x direction	1.2812E-02	1.6046E-02	1.8404E-02
	1.0208E-07	1.1747E-02	2.5056E-02
Taper in y direction	1.2812E-02	1.6062E-02	2.0683E-02
	1.0208E-07	1.1755E-02	2.9038E-02
Skew	9.2660E-02	0.1370	0.1650
	1.3143E-07	1.5006E-02	0.1330
Aspect ratio	1.2409	1.2812	1.1564
	1.1095	1.0818	1.2533

Note: Two averages are given for each distortion parameter. The first row gives an average for the entire mesh, and the second row gives an average value of the boundary elements in contact with the moving die.

Table 4 Average Distortion Parameters in Center Punch Forging of New Mesh after Time Step 41

Distortion parameter	Lagrange	Hermite	Poisson
Taper in x direction	3.1975E-02	3.5504E-02	4.2966E-02
	7.9204E-02	7.6128E-02	0.1733
Taper in y direction	2.8178E-02	2.9628E-02	3.8091E-02
	8.2023E-02	7.5409E-02	0.1475
Skew	0.4218	0.4536	0.3940
	0.1080	0.2472	0.6148
Aspect ratio	1.4626	1.4990	1.3042
	1.6978	1.5830	1.4995

Note: Two averages are given for each distortion parameter. The first row gives an average for the entire mesh, and the second row gives an average value of the boundary elements in contact with the moving die.

Table 5 Average Distortion Parameters in H-section Preform after Time Step 191

Distortion parameter	Lagrange	Hermite	Poisson
Taper in x direction	3.2675E-02	3.3357E-02	5.4876E-02
	0.0428	0.0415	0.1453
Taper in y direction	2.9242E-02	2.9909E-02	5.0660E-02
	0.0425	0.0421	0.1344
Skew	0.2095	0.2121	0.2544
	0.2940	0.3101	0.4895
Aspect ratio	1.8447	1.8449	1.7908
	1.7894	1.7776	1.7902

Note: Two averages are given for each distortion parameter. The first row gives an average for the entire mesh, and the second row gives an average value of the boundary elements in contact with the moving die.

Unlike the first two cases, both the stress contour plots and the elemental stresses obtained using different methods show a considerable difference between the results obtained using Poisson's mesh and the ones obtained using algebraic interpolation methods. The difference in the elemental stress values is significant and is as high as 200% in the extreme case.

6. Effect of Elemental Distortion on Finite-Element Solutions

Tables 2 through 5 present average distortion parameter values for four different meshes—(1) initial mesh for cylinder upsetting, (2) initial mesh for center punch forging, (3) new mesh for center punch forging after remeshing at the 41st step, and (4) new mesh for H-section preform after remeshing at the 191st time step. The distortion parameters presented are (1) taper in x direction, (2) taper in y direction, (3) skew, and (4) aspect ratio. Definitions of these parameters can be found in Ref 24. The aspect ratio of the elements does not affect the solution accuracy to a great extent.[25] Also, the aspect ratios in all the cases are comparable in value. For this reason, the following discussion takes into account only the other three parameters and does not focus on the effect of aspect ratio.

A review of the finite-element results presented in the previous section together with the corresponding distortion parameter tables clearly demonstrate the correlation between the distortion in the boundary elements in contact with the moving die and the solution accuracy. The boundary element distortion affects not only the stresses in boundary elements, but also the entire stress distribution pattern in the billet, as observed in H-section preform analysis. The results give an idea of the order of the critical magnitudes of the distortion parameters. The results for the first two cases (Fig. 5, 6, 10, and 11 and Tables 2 and 3) indicate that, if the difference in the distortion parameter values is of the order of 10^{-2}, it does not result in a significant difference in the solutions. On the other hand, magnitudes more than 10^{-1}, as in Tables 3 and 4, are found to introduce a considerable deviation in the results.

The average distortion parameter values for the entire mesh are found to be a poor indicator of the mesh quality, and this confirms the findings of another study[26] regarding the effect of element distortion on finite-element solutions. This is indicated by the center punch forging results presented in Fig. 13 and 14 and the average distortion values given in Table 4. These results also indicate that the stress contour plots alone cannot be used to make a fair comparison between two finite-element solutions. The stress contour plots in this case would indicate that all the three solutions are in a fair agreement with each other, when, in fact, the forging loads show a significant deviation. Another important factor that has an equal bearing on the accuracy of finite-element solutions is mesh densities. Although this

point is not fully addressed in this article, the authors would like to make the following remarks regarding this issue. The analysis was performed for two different mesh configurations in the case of cylinder upsetting, as well as center punch forging. In each case, both configurations were found to yield similar results. The results for center punch forging after remeshing show very high strain gradients between neighboring elements (Fig. 13), and the effect of mesh distortion might be less severe for a finer mesh. H-section preform analysis results show that the interelement strain rate gradient is quite low for most of the elements, and results are not expected to improve with an increase in the mesh density.

7. Concluding Remarks

The objective of this research was to identify a suitable approach toward mesh generation for the finite-element simulation of bulk metal-forming processes and test it by implementing it into CFORM. After a review of the current mesh generation methods and the specific requirements imposed by the forging design process, a knowledge-based approach, combined with the use of parametric mapping techniques, was selected for implementation. The reasons for making this choice have been stated in the introductory section. The input to this system consists of the description of boundary segments and vertices, together with the specification of the number of nodes on each segment. The mesh density distribution can be controlled by a proper placement of the boundary nodes. The final output of the system consists of the nodal coordinates and nodal connectivity arrays. Graphics interface has been developed in HOOPS, which allow the analyst to check the mesh at each stage of mesh generation. The mesh generation system has been successfully used in a number of forging problems and has been found to reduce the preprocessing time to a great extent.

Three mapping methods (described in Section 3) were used to generate the final meshes. The differences between the three methods were found to be very small. However, Lagrange interpolation was found to be the most suitable in terms of element distortion and computational time. The results presented in this article are not successful in isolating the effect of taper and skew on the solution accuracy, but they do provide an estimate of their critical magnitudes.

Presently, the mesh generation system is not fully automatic, but a skeleton or a basic framework has been programmed, which can be used to build a more sophisticated system. Work is being done to fully automate both—the mesh generation as well as remeshing, using the knowledge derived from the results obtained in different forging simulations.

References

1. I. Haque, J.E. Jackson, A.A. Tseng, and J.L. Rose, Ed., *Friction and Material Characterization*, MD-Vol 10, ASME, Dec (1988).
2. G. Weber and L. Anand, Finite Deformation Constitutive Equations and a Time Integration Procedures for Isotropic, Hyperelastic-Viscoplastic Solids, in *Computer Methods in Applied Mechanics and Engineering 79*, North Holland, New York, 173-202 (1990).
3. T.J.R. Hughes and J. Winget, Finite Rotation Effects in Numerical Integration of Rate Constitutive Equations, *Int. J. Num. Meth. Eng., 15*, 1862-1867 (1980).
4. J.E. Jackson, I. Haque, A. York, and N. Cherukury, The CFORM Computer Aided Forging Design Process, *Proc. ASME International Conference on Computers in Mechanical Engineering*, San Francisco, 335-342, Aug (1988).
5. W.T. Wu and S.I. Oh, "ALPIDT: A General Purpose FEM Code for Simulation of Nonisothermal Forming Processes", Thirteenth NAMRC Conference, Berkeley (1985).
6. M. Ramesh, A Finite Element Model for Short Fiber Composites Manufactured by Powder Metallurgy Techniques, unpublished Ph.D. dissertation, Mechanical Engineering Department, Clemson University.
7. R.D. Henshell, D. Walters, and G.B. Warburton, A New Family of Curvilinear Plate Bending Elements for Vibration and Stability, *J. Sound Vib., 20*, 381-397 (1972).
8. K. Ho-Le, Finite Element Mesh Generation Methods: A Review and a Classification, *Computer Aided Design, 20*, 27-38, Jan/Feb (1988).
9. M.S. Shephard, Approaches to the Automatic Mesh Generation and Control of Finite Element Meshes, *Appl. Mech. Rev., 41*(4), ASME Book No. AMR035, 169-185, Apr (1988).
10. J.C. Cavendish, Automatic Triangulation of Arbitrary Planer Domains for the Finite Element Method, *Int. J. Num. Meth. Eng., 8*, 679-696 (1974).
11. S.H. Lo, A New Mesh Generation Scheme for Arbitrary Planer Domains, *Int. J. Num. Meth., 21*, 1403-1426 (1985).
12. M.L.C. Sluiter and D.C. Hansen, A General Purpose Automatic Mesh Generator for Shell and Solid Finite Elements, *Computers in Engineering, 3*, 29-34 (1982).
13. A. Jain, Modern Methods for Automatic FE Mesh Generation, Modern Methods for Automating Finite Element Mesh Generation, *Proc. Nat. Convention of ASCE*, 19-28, Chicago, IL, Oct (1986).
14. P.L. Baehamann, L.W. Scott, M. Shephard, K.R. Grice, and M.A. Yerry, Robust Geometrically Based Automatic Two Dimensional Mesh Generation, *Int. J. Num. Meth. Eng., 24*, 1043-1078 (1987).
15. A. Kela, R. Perucchio, and H. Volecker, Toward Automatic Finite Element Analysis, *Comp. Mech. Eng.*, Jul, 57-71 (1986).
16. T.D. Blacker, M.B. Stephenson, J.L. Mitchiner, L.R. Philips, and Y.T. Lin,"Automated Quadrilateral Mesh Generation: A Knowledge System Approach," 88-WA/CIE4, ASME Winter Annual Meeting, Chicago, IL, Dec (1988).
17. M.B. Blacker, J.L. Mitchiner, L.R. Philips, and Y.T. Lin, Knowledge System Approach to Automated Two Dimensional Quadrilateral Mesh Generation, ASME Int. Comp. Eng. Conference, San Francisco, 153-162, Jul (1988).
18. P.D. Dabke, A Knowledge-Based System for Automating Finite Element Mesh Generation in CFORM, Master's thesis, Engineering Mechanics, Clemson University, May (1991).
19. E.A. Siebler, Object Oriented Programming in PROLOG, *AI Expert*, 46-57, Oct (1986).
20. J. R. Walters and N.R. Nielsen, *Crafting Knowledge Based Systems/Expert Systems Made Realistic*, John Wiley & Sons, New York (1988).
21. J. Thompson, Z.U.A. Warsi, and W. Mastin, *Numerical Grid Generation: Foundation and Applications*, North Holland, New York (1985).
22. C.H. Lee and S. Kobayashi, New Solutions to Rigid Plastic Deformation Problems Using a Matrix Method, *J. Eng. Ind., 95*, 865-873 (1973).

23. B. Lamm, J.E. Jackson, and I. Haque, "Feasibility Design of Axisymmetric Center Punch Forging by Finite Element Method," Technical Report, Mechanical Engineering Dept., Clemson University, Jul (1988).
24. J. Robinson, Some New Distortion Measures for Quadrilaterals, *Finite Element in Analysis and Design,* Vol 3, 183-197 (1987).
25. A.R. York, "A Study of Remeshing Procedures for Large Plane Strain Problems with Specific Application to the CFORM-FEM Computer Code," Master's thesis, Mechanical Engineering Dept., Clemson University, May (1988).
26. M. Srikrishna, "A Knowledge-Based System for Automating Remeshing Procedures in Metal Forming Simulations," unpublished Master's thesis, Mechanical Engineering Dept., Clemson University, Dec (1991).